Appl Phys B (2011) 103:897–906
DOI 10.1007/s00340-011-4439-x

Applied Physics B
Lasers and Optics

Extending the zero-effective-phase photonic bandgap by one-dimensional ternary photonic crystals

Y. Xiang · X. Dai · S. Wen · Z. Tang · D. Fan

Received: 22 August 2010 / Revised version: 10 January 2011 / Published online: 26 February 2011

Abstract A novel method to enlarge the zero-effective-phase bandgap has been presented in the one-dimensional photonic crystals by sandwiching the third material between the two single-negative materials to form a one-dimensional ternary periodic structure. The band-edges formula for the one-dimensional ternary photonic crystal is derived based on the effective-medium theory and the expressions of the upper and lower frequency limits for the ternary photonic crystals are obtained. Then two schemes to enlarge the zero-effective-phase bandgaps are put forward. Moreover, the angular- and polarization-dependences of the photonic bandgap are investigated. Finally, the role of the dispersion in the sandwiched layer on the bandgap extending has been discussed and two schemes are also presented to enlarge the zero-effective-phase photonic bandgap.

1 Introduction

Photonic crystals (PCs) have attracted much attention over the past decades [1, 2], which can generate spectral regions named photonic bandgap (PBG). Electromagnetic waves with frequencies falling within PBG cannot propagate through the PCs. There exists the omnidirectional PBG in some specific structure, which can reflect electromagnetic waves incidenting at any angle with any polarization [3–6]. One-dimensional photonic crystals (1DPCs) composed of alternating layers of positive-index materials (PIMs) and negative-index metamaterials (NIMs) [7–9] possess zero-average-index (zero-$\bar{n}$) PBG [10–14]. It is also found that stacking alternating layers of Epsilon-negative (ENG) materials and Mu-negative (MNG) materials will lead to a zero-effective-phase (zero-φ_{eff}) PBG [15–17]. Both zero-$\bar{n}$ and zero-φ_{eff} PBGs are omnidirectional PBGs; the properties (the central frequency and the width) of these PBGs are invariant upon the change of scaling and are insensitive to the disorder, which are also independent on the incident angles and polarizations. The defect modes inside these gaps are insensitive to the incident angle [16]. Zero-$\bar{n}$ and zero-φ_{eff} PBGs are fundamentally different from the usual PBGs induced by the Bragg scattering (Bragg gaps), which have potential applications in improving omnidirectional mirrors [18], omnidirectional optical filters [19], and optical switches [20], etc.

It has been demonstrated by some authors that the frequency range of the omnidirectional zero-$\bar{n}$ PBG can be enhanced by combining two or more 1D binary PCs (photonic heterostructures) [13, 21]. Recently, enlarging the zero-$\bar{n}$ bandgap frequency range in one-dimensional ternary PC (three material layers constituting a period of the lattice) is also presented [22]. However, the schemes to enhance frequency range of the zero-φ_{eff} PBG are still absent, and there are a few papers discussing how to enlarge this omnidirectional reflection band. In this paper, we report an approach to enlarge the omnidirectional frequency range of the zero-φ_{eff} gap by sandwiching another layer between the alternating layers of two different single-negative (SNG) materials.

Y. Xiang (✉) · S. Wen · Z. Tang · D. Fan
Laboratory for Micro/Nano Optoelectronic Devices of Ministry of Education, School of Information Science and Engineering, Hunan University, Changsha 410082, China
e-mail: xiangyuanjiang@126.com

S. Wen (✉)
e-mail: scwen@vip.sina.com
Fax: +86-731-88823474

X. Dai
College of Electrical and Information Engineering, Hunan University, Changsha 410082, China

In this one-dimensional ternary PC, it is found that the frequency range of the zero-φ_{eff} gap can be enhanced remarkably compared to the original binary PCs.

Our study has been carried out in three steps. Firstly, in Sect. 2, the frequency limits for the upper and lower band-edges of the zero-φ_{eff} PBG in the one-dimensional ternary PC are obtained based on the effective medium theory. Then in Sect. 3, we investigate systemically the properties of omnidirectional zero-φ_{eff} PBG in this one-dimensional ternary PC by using the photonic band-edges formula, and a novel method to extend zero-φ_{eff} PBGs is proposed. The results obtained are summarized in Sect. 4.

2 Basic equations and numerical method

2.1 Transfer-matrix method and the dispersion relation

The one-dimensional binary PC $(\text{AB})^{\text{M}}$ is formed by alternating layers of two different materials (A and B). For the zero-$\bar{n}$ bandgap, the layers A and B are PIMs and NIMs respectively; for the zero-φ_{eff} bandgap, the layers A and B are ENG material and MNG material, respectively. The one-dimensional ternary PC $(\text{ACB})^{\text{M}}$ is constructed by sandwiching a thin layer of a third material C between the two layers of the binary structure periodically (Fig. 1). We assume that the thickness of the medium $A(\varepsilon_a, \mu_a)$, medium $B(\varepsilon_b, \mu_b)$ and medium $C(\varepsilon_c, \mu_c)$ are d_A, d_B, and d_C, respectively. And $d = d_A + d_B + d_C$ is the period of the unit cell, M is the number of periods.

We use the transfer-matrix method (TMM) [23] to identify the transmittance spectra of the structure. Let a plane wave be incident from vacuum at an angle θ onto the 1DPC with $+z$ direction. Generally, the electric and magnetic fields at any two positions z and $z + \Delta z$ in the same layer can be related via a transfer matrix [23],

$$M(\Delta z, \omega) = \begin{pmatrix} \cos(k_{iz}\Delta z) & -\frac{1}{q_{iz}}\sin(k_{iz}\Delta z) \\ q_{iz}\sin(k_{iz}\Delta z) & \cos(k_{iz}\Delta z) \end{pmatrix}, \tag{1}$$

where $i = A, B, C$ denote different layers, and $k_{iz} = (\omega/c)\sqrt{\varepsilon_i}\sqrt{\mu_i}\sqrt{1 - \sin^2\theta/\varepsilon_i\mu_i}$ is the components of the wave vector along the z axis in the medium, $q_{iz} = \sqrt{\varepsilon_i}/\sqrt{\mu_i}\sqrt{1 - \sin^2\theta/\varepsilon_i\mu_i}$ for the TE-mode, and $q_{iz} = \sqrt{\mu_i}/\sqrt{\varepsilon_i}\sqrt{1 - \sin^2\theta/\varepsilon_i\mu_i}$ for the TM-mode, c is the vacuum speed of light. The total transfer matrix connecting the field at the incident end and the exit end can be written as

$$X(\omega) = \prod_{i=1}^{2M} M_i(\Delta z, \omega) = \begin{pmatrix} x_{11}(\omega) & x_{12}(\omega) \\ x_{21}(\omega) & x_{22}(\omega) \end{pmatrix}. \tag{2}$$

Then the transmission coefficient $t(\omega)$ can be obtained from the TMM [23],

$$t(\omega) = \frac{2q_0}{[q_0 x_{22}(\omega) + q_s x_{11}(\omega)] - j[q_0 q_s x_{12}(\omega) - x_{21}(\omega)]}. \tag{3}$$

Here, $q_0 = q_s = \cos\theta$ for the vacuum of the space $z < 0$ before the incident end and the space $z > L$ after the exit end, where L is the total length of the 1DPC; $x_{ij}(\omega)$ $(i, j = 1, 2)$ are the matrix elements of $X(\omega)$, j denotes the imaginary unit.

Moreover, for an infinite periodic structure $(M \to \infty)$, based on the Bloch's condition $\varphi(z + d) = \exp(jKd)\varphi(z)$ and the boundary condition, the dispersion relation for any incident angle follows that [24]

$$\begin{aligned} \cos(Kd) = {} & \cos(k_{Az}d_A)\cos(k_{Bz}d_B)\cos(k_{Cz}d_C) \\ & - \frac{1}{2}\left(\frac{q_{Az}}{q_{Bz}} + \frac{q_{Bz}}{q_{Az}}\right) \\ & \times \sin(k_{Az}d_A)\sin(k_{Bz}d_B)\cos(k_{Cz}d_C) \\ & - \frac{1}{2}\left(\frac{q_{Az}}{q_{Cz}} + \frac{q_{Cz}}{q_{Az}}\right)\sin(k_{Az}d_A) \\ & \times \cos(k_{Bz}d_B)\sin(k_{Cz}d_C) \\ & - \frac{1}{2}\left(\frac{q_{Bz}}{q_{Cz}} + \frac{q_{Cz}}{q_{Bz}}\right) \\ & \times \cos(k_{Az}d_A)\sin(k_{Bz}d_B)\sin(k_{Cz}d_C). \end{aligned} \tag{4}$$

For the binary PCs, we can assume that $d_C = 0$, then the dispersion relation can be recovered to the following form [24]:

$$\begin{aligned} \cos(Kd) = {} & \cos(k_{Az}d_A)\cos(k_{Bz}d_B) \\ & - \frac{1}{2}\left(\frac{q_{Az}}{q_{Bz}} + \frac{q_{Bz}}{q_{Az}}\right)\sin(k_{Az}d_A)\sin(k_{bz}d_B), \end{aligned} \tag{5}$$

which has been discussed in plenty of work [15, 16] where K is the z component of Bloch wave-vector. For a real K, the Bloch waves are propagating, but a complex K indicates the presence of PBGs, where the wave propagation is inhibited. If the materials are SNG materials, then k_{iz} and q_{iz} are imaginary numbers. Hence, $k_{iz} = j|k_{iz}|$ and $q_{iz} = j|q_{iz}|$,

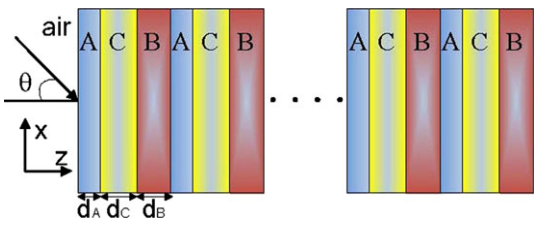

Fig. 1 Schematic of a one-dimensional ternary photonic crystal $[\text{ACB}]^{\text{M}}$ constructed by sandwiching the layer C between the alternating layers of material A and material B in the air background

we can use the relation $\cos(i|k_{iz}|d_i) = \cosh(|k_{iz}|d_i)$ and $\sin(i|k_{iz}|d_i) = i\sinh(|k_{iz}|d_i)$, then the transfer matrix and dispersion relation can be transformed to the corresponding equations for the SNG materials.

2.2 Effective-medium theory and the location of the photonic bandgap edges

The transfer matrices of the each layer are as the following:

$$M_A(d_A,\omega) = \begin{pmatrix} \cos(k_{Az}d_A) & -\frac{1}{q_{Az}}\sin(k_{Az}d_A) \\ q_{Az}\sin(k_{Az}d_A) & \cos(k_{Az}d_A) \end{pmatrix},$$
$$M_B(d_B,\omega) = \begin{pmatrix} \cos(k_{Bz}d_B) & -\frac{1}{q_{Bz}}\sin(k_{Bz}d_B) \\ q_{Bz}\sin(k_{Bz}d_B) & \cos(k_{Bz}d_B) \end{pmatrix}, \quad (6)$$
$$M_C(d_C,\omega) = \begin{pmatrix} \cos(k_{Cz}d_C) & -\frac{1}{q_{Cz}}\sin(k_{Cz}d_C) \\ q_{Cz}\sin(k_{Cz}d_C) & \cos(k_{Cz}d_C) \end{pmatrix},$$

It is evident that in the subwavelength limit, the product of the wave vector k_{iz} and the thicknesses of the layers Δz $(=d_A, d_B, d_C)$ generally satisfy the condition $k_{iz}\Delta z \ll 1$. As a result, we have $\sin(k_{iz}\Delta z) \approx k_{iz}\Delta z$ and $\cos(k_{iz}\Delta z) \approx 1$. Then, for the TE polarization, the transfer matrix of every layer has the form,

$$M_A(d_A,\omega) \approx \begin{pmatrix} 1 & -\mu_A d_A(\omega/c) \\ -\frac{\omega}{c}\varepsilon_A(1-\frac{\sin^2\theta}{\varepsilon_A\mu_A})d_A & 1 \end{pmatrix},$$
$$M_B(d_B,\omega) \approx \begin{pmatrix} 1 & -\mu_B d_B(\omega/c) \\ -\frac{\omega}{c}\varepsilon_B(1-\frac{\sin^2\theta}{\varepsilon_B\mu_B})d_B & 1 \end{pmatrix}, \quad (7)$$
$$M_C(d_C,\omega) \approx \begin{pmatrix} 1 & -\mu_C d_C(\omega/c) \\ -\frac{\omega}{c}\varepsilon_C(1-\frac{\sin^2\theta}{\varepsilon_C\mu_C})d_C & 1 \end{pmatrix}.$$

The total transfer matrices for the unit cell can be written as

$$M_d(d,\omega) = M_A(d_A,\omega)M_B(d_B,\omega)M_C(d_C,\omega)$$
$$\approx \begin{pmatrix} 1 & -\frac{\omega}{c}d(\mu_A f_A + \mu_B f_B + \mu_C f_C) \\ \frac{\omega}{c}d[(\varepsilon_A f_A + \varepsilon_B f_B + \varepsilon_C f_C) + \sin^2\theta(\frac{f_A}{\mu_A} + \frac{f_B}{\mu_B} + \frac{f_C}{\mu_C})] & 1 \end{pmatrix} \quad (8)$$

where $f_A = d_A/d$, $f_B = d_B/d$, $f_C = d_C/d$, $d = d_A + d_B + d_C$.

On the other hand, since the layered structure has an anisotropic electromagnetic property, we can assume that the effective slab has the effective permittivity and permeability to be anisotropic and have the diagonalizable forms as follows [25, 26],

$$\varepsilon_{\text{eff}} = \begin{pmatrix} \varepsilon_{\text{eff}x} & 0 & 0 \\ 0 & \varepsilon_{\text{eff}y} & 0 \\ 0 & 0 & \varepsilon_{\text{eff}z} \end{pmatrix},$$
$$\mu_{\text{eff}} = \begin{pmatrix} \mu_{\text{eff}x} & 0 & 0 \\ 0 & \mu_{\text{eff}y} & 0 \\ 0 & 0 & \mu_{\text{eff}z} \end{pmatrix}. \quad (9)$$

When the electromagnetic wave is propagating in the effective slab, the effective wave vector for the TE polarization can be determined by the following equation:

$$k^2_{\text{eff}z} = \varepsilon_{\text{eff}y}\mu_{\text{eff}x}\frac{\omega^2}{c^2} - \frac{\mu_{\text{eff}x}}{\mu_{\text{eff}z}}k^2_{\text{eff}x}, \quad (10a)$$

and

$$k^2_{\text{eff}z} = \mu_{\text{eff}y}\varepsilon_{\text{eff}x}\frac{\omega^2}{c^2} - \frac{\varepsilon_{\text{eff}x}}{\varepsilon_{\text{eff}z}}k^2_{\text{eff}x}, \quad (10b)$$

for the TM polarization, where $k^2_{\text{eff}x}$ can also be written as $k^2_{\text{eff}x} = (\omega^2/c^2)\sin^2\theta$, and in the subwavelength limit, the effective transfer matrix of the effective slab is:

$$M_{\text{eff}}(d,\omega) = \begin{pmatrix} \cos(k_{\text{eff}z}d) & -\frac{1}{q_{\text{eff}z}}\sin(k_{\text{eff}z}d) \\ q_{\text{eff}z}\sin(k_{az}d) & \cos(k_{\text{eff}z}d) \end{pmatrix}$$
$$\approx \begin{pmatrix} 1 & -\mu_{\text{eff}x}d(\omega/c) \\ (\omega/c)\varepsilon_{\text{eff}y}(1-\frac{\sin^2\theta}{\varepsilon_{\text{eff}y}\mu_{\text{eff}z}})d & 1 \end{pmatrix}, \quad (11)$$

where $k_{\text{eff}z} = (\omega/c)\sqrt{\varepsilon_{\text{eff}x}}\sqrt{\mu_{\text{eff}y}}\sqrt{1-\sin^2\theta/\varepsilon_{\text{eff}z}\mu_{\text{eff}y}}$ are the components of the wave vector along the z axis in the medium, $q_{\text{eff}z} = \sqrt{\varepsilon_{\text{eff}x}}/\sqrt{\mu_{\text{eff}y}}\sqrt{1-\sin^2\theta/\varepsilon_{\text{eff}z}\mu_{\text{eff}y}}$ for the TE-mode.

Comparing (8) with (11), we then get the three elements of the effective permittivity and permeability tensors of the unit cell,

$$\mu_{\text{eff}x} = \mu_A f_A + \mu_B f_B + \mu_C f_C,$$
$$\varepsilon_{\text{eff}y} = \varepsilon_A f_A + \varepsilon_B f_B + \varepsilon_C f_C, \quad (12)$$
$$\mu_{\text{eff}z} = 1\Big/\left(\frac{f_A}{\mu_A} + \frac{f_B}{\mu_B} + \frac{f_C}{\mu_C}\right).$$

As for the TM mode case, we just need to make a substitution of $\varepsilon \leftrightarrow \mu$. Then the other three effective elements can be obtained

$$\begin{aligned}
\varepsilon_{\mathrm{eff}x} &= \varepsilon_A f_A + \varepsilon_B f_B + \varepsilon_C f_C, \\
\mu_{\mathrm{eff}y} &= \mu_A f_A + \mu_B f_B + \mu_C f_C, \\
\varepsilon_{\mathrm{eff}z} &= 1 \Big/ \left(\frac{f_A}{\varepsilon_A} + \frac{f_B}{\varepsilon_B} + \frac{f_C}{\varepsilon_C} \right).
\end{aligned} \tag{13}$$

In the effective slab, when the effective wave vectors $k^2_{\mathrm{eff}z} > 0$, the waves can propagate in the medium; on the contrary, when $k^2_{\mathrm{eff}z} < 0$, $k_{\mathrm{eff}z}$ is an imaginary number, hence waves cannot propagate in the medium, then the PBG will exist. Hence, the conditions for the PBG edges can be written as

$$k^2_{\mathrm{eff}z} = 0. \tag{14}$$

Combined (10) and (14), we can obtain the photonic band-edges formula as the following expressions:

$$\bar{\varepsilon} - \overline{\mu^{-1}} \sin^2\theta = 0 \quad \text{and} \quad \bar{\mu} = 0 \tag{15}$$

for the TE polarization, and

$$\bar{\varepsilon} = 0 \quad \text{and} \quad \bar{\mu} - \overline{\varepsilon^{-1}} \sin^2\theta = 0 \tag{16}$$

for the TM polarization, where $\bar{\mu} = \mu_A f_A + \mu_B f_B + \mu_C f_C$, $\bar{\varepsilon} = \varepsilon_A f_A + \varepsilon_B f_B + \varepsilon_C f_C$, $\overline{\mu^{-1}} = \frac{f_A}{\mu_A} + \frac{f_B}{\mu_B} + \frac{f_C}{\mu_C}$ and $\overline{\varepsilon^{-1}} = \frac{f_A}{\varepsilon_A} + \frac{f_B}{\varepsilon_B} + \frac{f_C}{\varepsilon_C}$.

For the normal incidence, $\theta = 0$, hence the frequency locations of the PBGs edges for both polarizations can be simplified as

$$\bar{\varepsilon} = 0 \quad \text{and} \quad \bar{\mu} = 0. \tag{17}$$

When the structure is binary PC, we can set $f_c = 0$, then the band-edges formula will restore to the formula for the binary PC in the zero-φ_{eff} or zero-$\bar{n}$ PBGs [27, 28].

The band-edges formula (15)–(17) can apply to the zero-φ_{eff} or zero-$\bar{n}$ PBGs. When only one of the conditions holds, the conditions at the normal incidence should become

$$\bar{\varepsilon} = 0 \quad \text{or} \quad \bar{\mu} = 0 \tag{18}$$

$\bar{\varepsilon} = 0$ for the ENG materials and $\bar{\mu} = 0$ for the MNG materials.

3 Results and discussions

In the present paper, we discuss how to enlarge the zero-φ_{eff} PBGs, hence it is assumed that A is ENG material, B is MNG material, and layer C maybe the PIM, NIM and SNG material. We adopt the Drude model to descript the dispersion dielectric permittivity and magnetic permeability of the SNG material,

$$\varepsilon_A = \varepsilon_1 - \frac{\alpha}{\omega^2}, \qquad \mu_A = \mu_1, \tag{19}$$

and

$$\varepsilon_B = \varepsilon_2, \qquad \mu_B = \mu_2 - \frac{\beta}{\omega^2}. \tag{20}$$

Here, we have neglected the losses because we just want to discuss the methods of the enlargement of the zero-φ_{eff} PBGs principally, in general, the losses will change the intensity peak of the transmission or reflection coefficient and, however, it cannot change the fundamental properties of the zero-φ_{eff} PBGs.

For the normal incidence, according to (17), the band-edges frequencies can be written as

$$\omega_1\ (\bar{\varepsilon} = 0) = \sqrt{\frac{\alpha}{\varepsilon_1 + (d_B/d_A)\varepsilon_2 + (d_C/d_A)\varepsilon_3}}, \tag{21a}$$

$$\omega_2\ (\bar{\mu} = 0) = \sqrt{\frac{\beta}{\mu_2 + (d_A/d_B)\mu_1 + (d_C/d_B)\mu_3}}. \tag{21b}$$

Here, in order to simplify the problem, firstly, we have assumed that the layer C is nondispersive materials, $\varepsilon_C = \varepsilon_3$ and $\mu_C = \mu_3$. When $d_C = 0$, the band-edges frequencies can be recovered to the corresponding relations in the binary PCs containing two different SNG materials:

$$\omega_1\ (\bar{\varepsilon} = 0) = \sqrt{\frac{\alpha}{\varepsilon_1 + (d_B/d_A)\varepsilon_2}}, \tag{22a}$$

$$\omega_2\ (\bar{\mu} = 0) = \sqrt{\frac{\beta}{\mu_2 + (d_A/d_B)\mu_1}}. \tag{22b}$$

If $\omega_1 < \omega_2$, ω_1 is the lower frequency band-edge and ω_2 is the upper frequency band-edge; contrarily, ω_2 is the lower frequency band-edge and ω_1 is the upper frequency band-edge. The width of the zero-φ_{eff} PBGs can be written as

$$\Delta\omega = |\omega_2 - \omega_1|. \tag{23}$$

The bigger difference between ω_1 and ω_2 is, the larger bandwidth $\Delta\omega$ can be gotten. By comparing (21) with (22), it is found that increasing or decreasing the thickness d_C are not very effective for enlarging zero-φ_{eff} PBG when ε_3 and μ_3 have identical signs, in this sense ω_1 and ω_2 will increase or decrease at the same time. The situation is similar for increasing or decreasing ε_3 and μ_3 with the same sign. To enlarge the width of the zero-φ_{eff} PBG remarkably in the ternary 1DPC, we adopt the following schemes according to (21)–(23):

(1) when $\omega_1 < \omega_2$, to obtain a larger width $\Delta\omega$, we set $\varepsilon_3 > 0$ and $\mu_3 < 0$;
(2) when $\omega_1 > \omega_2$, to obtain a larger width $\Delta\omega$, we set $\varepsilon_3 < 0$ and $\mu_3 > 0$.

In the following numerical calculations, we assume that $\varepsilon_1 = \mu_2 = 1$, $\varepsilon_2 = \mu_1 = 3$, and $\alpha = \beta = 100$ (GHz^2), $d_A = 12$ mm, and have neglected the loss in the simulations.

3.1 Normal incidence

First, we discuss the PBG of the binary PCs containing two different SNG materials, the projected band structure at the normal incidence obtained from the TMM is plotted as a function of the frequency and thickness ratio d_B/d_A in the Fig. 2, where $d_A = 12$ mm. It is clear that the point of intersection exists at $\omega_1 = \omega_2 = 5$ GHz when $d_A = d_B$. Furthermore, if $d_B < d_A$, then $\omega_1 > \omega_2$, hence ω_1 is the upper frequency band-edge and ω_2 is the lower frequency band-edge; but as d_B/d_A is increasing, when $d_B > d_A$, ω_1 becomes the lower frequency band-edge and ω_2 turns into the upper frequency band-edge. Also, it is shown that the band-edges frequencies obtained by the band-edge formula agree well with the results in the TMM.

Next, we consider two kinds of cases. For the first case, we choose $d_B = 6$ mm. In this case, $\omega_1 > \omega_2$, according to the Scheme (2), we set $\varepsilon_3 = -3$, $\mu_3 = 1$, and $d_C = 6$ mm, the transmittance spectrum of the 1DPC $(\mathrm{ACB})^{\mathrm{M}}$ has been shown in Fig. 3(a). For the another case, the thickness of the material B' is larger than the thickness of the material A, we assume $d_B = 24$ mm, hence $\omega_1 < \omega_2$, according to the Scheme (1), we set $\varepsilon_3 = 1$, $\mu_3 = -3$, and $d_C = 6$ mm, the transmittance spectrum of the 1DPC $(\mathrm{ACB}')^{\mathrm{M}}$ is shown in Fig. 3(b). To be convenient for comparison, we also plot the transmittance spectra for the binary PCs [$(\mathrm{AB})^{\mathrm{M}}$ or $(\mathrm{AB}')^{\mathrm{M}}$] in the corresponding figures. For the first case, the bandwidth of the binary PC $(\mathrm{AB})^{\mathrm{M}}$ is $\Delta\omega = 2.65$ GHz, and the bandwidth of the ternary PC $(\mathrm{ACB})^{\mathrm{M}}$ is $\Delta\omega = 6.3$ GHz. The bandwidth in the ternary PC has been extended to 2.38 times as that in the binary PC. However, for the second case, the bandwidth of the binary PC $(\mathrm{AB}')^{\mathrm{M}}$ is $\Delta\omega = 2.3$ GHz, and the bandwidth of the ternary PC $(\mathrm{ACB}')^{\mathrm{M}}$ is $\Delta\omega = 3.7$ GHz, the bandwidth in this ternary PC is the 1.61 times as that in the binary PC. Hence, our schemes for enhancing the width of the zero-φ_{eff} PBG are very effective.

Of course, the width can be extended continually. In the first case, it can be realized by increasing the absolute value of ε_3 or μ_3. Generally, increasing the upper frequency limit is more effective than decreasing the lower frequency limit for enlarging the bandwidth. Figure 4(a) shows the transmittance spectra for the first case when $\varepsilon_3 = -3$, -4 and -5, the corresponding dispersion relations are also given in the Fig. 4(b). It is clear that the gap widths have been enlarged when the absolute value of ε_3 increases. The in-

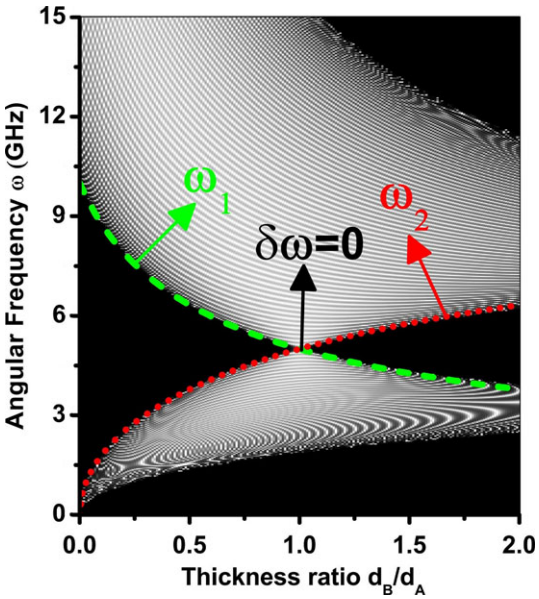

Fig. 2 The upper and lower frequencies limits obtained by the band-edges formulas at normal incidence, where the *dashed-line* is ω_1, the *dotted-line* is ω_2. For comparison, we also plotted the projected band structure obtained by TMM; the *black region* is the photonic bandgap. The parameters are $\varepsilon_1 = \mu_2 = 1$, $\varepsilon_2 = \mu_1 = 3$ and $\alpha = \beta = 100$ (GHz^2), $d_A = 12$ mm

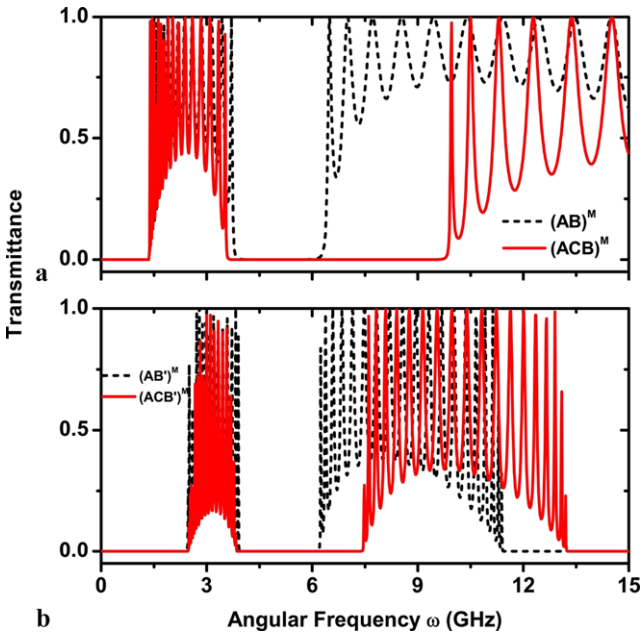

Fig. 3 Transmittance spectra for two different one-dimensional ternary photonic crystals are shown in *solid-line*. (**a**) $(\mathrm{ACB})^{\mathrm{M}}$, where $d_A = 12$ mm, $d_B = 6$ mm, $\varepsilon_3 = -3$, $\mu_3 = 1$, and $d_C = 6$ mm; (**b**) $(\mathrm{ACB}')^{\mathrm{M}}$, where $d_A = 12$ mm, $d_B = 24$ mm, $\varepsilon_3 = 1$, $\mu_3 = -3$, and $d_C = 6$ mm. To compare, the corresponding transmittance spectra for one-dimensional binary photonic crystals $(\mathrm{AB})^{\mathrm{M}}$ and $(\mathrm{AB}')^{\mathrm{M}}$ are also shown in *dashed-line*, where $M = 20$

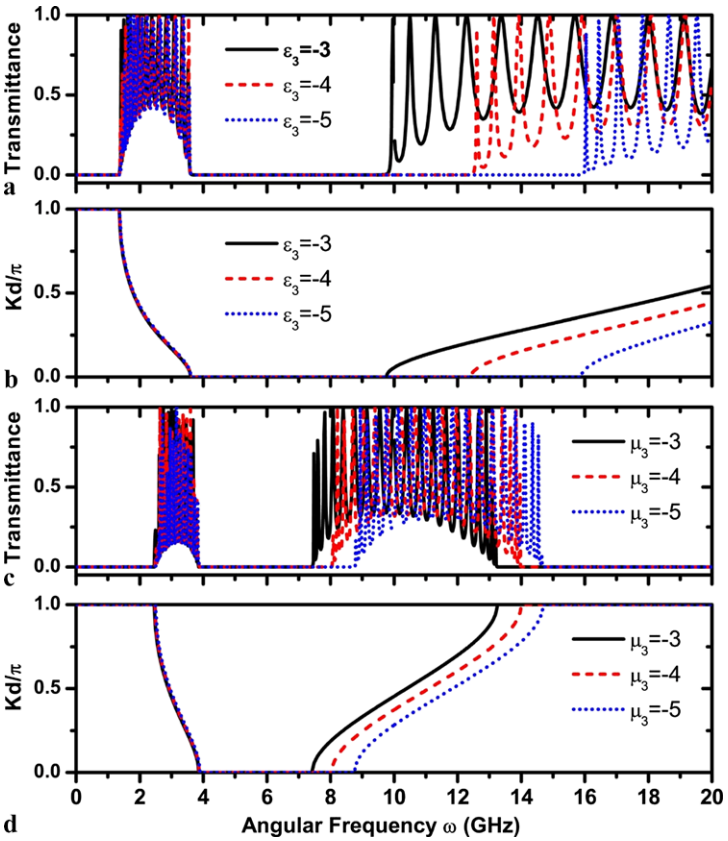

Fig. 4 Transmittance spectra and dispersion curves for two different one-dimensional ternary photonic crystals for different ε_3 or μ_3. (**a**) PC $(\mathrm{ACB})^{\mathrm{M}}$, where $d_A = 12$ mm, $d_B = 6$ mm, $\mu_3 = 1$, and $d_C = 6$ mm, $\varepsilon_3 = -3$ (*solid-line*), $\varepsilon_3 = -4$ (*dashed-line*), and $\varepsilon_3 = -5$ (*dotted-line*); (**b**) the corresponding dispersion relations for (**a**); (**c**) PC $(\mathrm{ACB}')^{\mathrm{M}}$, where $d_A = 12$ mm, $d_B = 24$ mm, $\varepsilon_3 = 1$, and $d_C = 6$ mm, $\mu_3 = -3$ (*solid-line*), $\mu_3 = -4$ (*dashed-line*), $\mu_3 = -5$ (*dotted-line*); (**d**) the corresponding dispersion relations for (**c**)

creases of absolute value of ε_3 makes the upper frequency limit shifts to higher frequency. However, the lower frequency limit is not moving due to the fixed $\mu_3 = 1$. For the second case, the gap widths can also be enlarged continually by increasing the absolute value of ε_3 or μ_3. Figure 4(c) shows the transmittance spectra when $= -3$, -4 and -5, the corresponding dispersion relations are given in the Fig. 4(d). The gap widths have been enhanced by increasing the absolute value of μ_3. It should be pointed out that the gap width in the first case is larger than that in the second case.

Moreover, through the analysis of (19), it is indicated that the gap widths will be extended by increasing the thickness of the layer C. Figure 5 shows the transmittance spectra and corresponding dispersion curves for the above two cases. For the first case (Figs. 5(a) and 5(b)), when the thickness of the layer C increases from 6 mm to 10 mm, the upper frequency limits moves to higher frequency remarkably, however, the lower frequency limits shifts to lower frequency slightly. For the second case (Figs. 5(c) and 5(d)), as the increases of the thickness of the layer C, the upper frequency limits also move to higher frequency, however, the magnitude of gap width variations is smaller than that in the first case by increasing d_C.

3.2 Oblique incidence

Up to now, we have just investigated the transmittance spectra and schemes to enlarge the gap width of the zero-φ_{eff} PBG at the normal incidence. However, the incident angle has strong effect on the gap width of the zero-φ_{eff} PBG. To get the gap width of the omnidirectional PBGs, we must consider the electromagnetic waves incident at any angle with any polarization. Next, we choose the first case as an example, and demonstrate that the omnidirectional PBGs are also been extended in the ternary PC. The results have been displayed in the Fig. 6. Figures 6(a) and 6(b) show the projected band structures for binary PCs $(\mathrm{AB})^{\mathrm{M}}$ for TE and TM polarization, respectively. To compare, the upper and lower frequency limits obtained by (15) and (16) are also shown in the Fig. 6. It is clear that the omnidirectional PBG width of $(\mathrm{AB})^{\mathrm{M}}$ is about $\Delta\omega_1 = 2.545$ GHz. Furthermore, Figs. 6(c) and 6(d) present the projected band structures for ternary PCs $(\mathrm{ACB})^{\mathrm{M}}$ for TE and TM polarization, respectively. It is found that the upper frequency limit of the TE polarization shifts to lower frequency remarkably, which has decreased the omnidirectional PBG width strongly. The omnidirectional PBG width of $(\mathrm{ACB})^{\mathrm{M}}$ is about $\Delta\omega_2 = 4.904$ GHz. The omnidirectional PBG width in the ternary PC is almost two times as the width in the binary PC $(\mathrm{AB})^{\mathrm{M}}$.

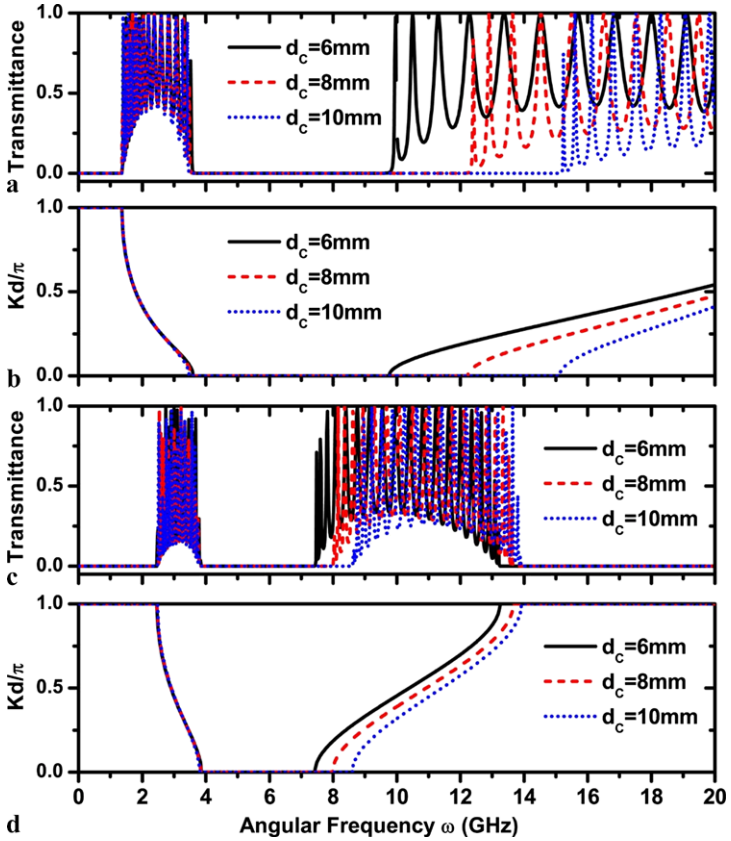

Fig. 5 Transmittance spectra and dispersion curves for two different one-dimensional ternary photonic crystals for different thickness of the layer C. (**a**) PC $(ACB)^M$, where $d_A = 12$ mm, $d_B = 6$ mm, $\mu_3 = 1$, and $\varepsilon_3 = -3$, (**b**) the corresponding dispersion relations for (**a**); (**c**) PC $(ACB')^M$, where $d_A = 12$ mm, $d_B = 24$ mm, $\varepsilon_3 = 1$, and $\mu_3 = -3$, (**d**) the corresponding dispersion relations for (**c**). In the figures, the *solid-line* is for $d_C = 6$ mm, the *dashed-line* is for $d_C = 8$ mm, the *dotted-line* is for $d_C = 10$ mm

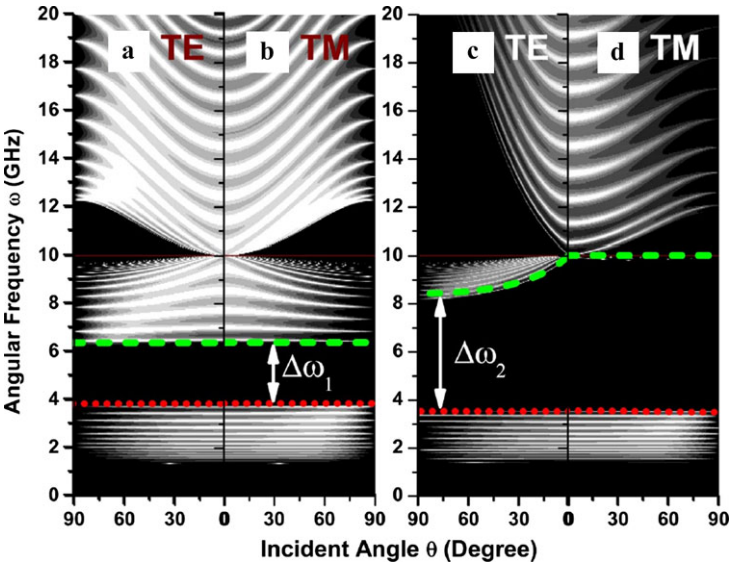

Fig. 6 (**a**) and (**b**) are the projected band structures for binary PC $(AB)^M$ of the TE polarization and TM polarization, respectively. (**c**) and (**d**) are the projected band structures for ternary PC $(ACB)^M$ of the TE polarization and TM polarization, respectively. The parameters have the same values as those in the Fig. 3(a). To compare, the upper and lower frequency limits obtained by the band-edges formula are also displayed in the figures, where the *dashed-line* is the upper frequency limit and the *dotted-line* is the lower frequency limit

3.3 Role of the dispersive permittivity and permeability in the material C on the bandgap extending

In the above discussion, the dispersions of the permittivity and permeability in the material C have been neglected. However, the dispersion of the metamaterials is inevitable. Next, we will discuss the role of the dispersions on the bandgap extending.

Now we assume that the material C is governed by the Durde model,

$$\varepsilon_C = \varepsilon_3 - \frac{\alpha'}{\omega^2}, \qquad \mu_C = \mu_3 - \frac{\beta'}{\omega^2}, \tag{24}$$

where α' and β' are the electric and magnetic plasma frequencies, and we consider that both ε_3 and μ_3 are positive constants. At the normal incidence, according to the pho-

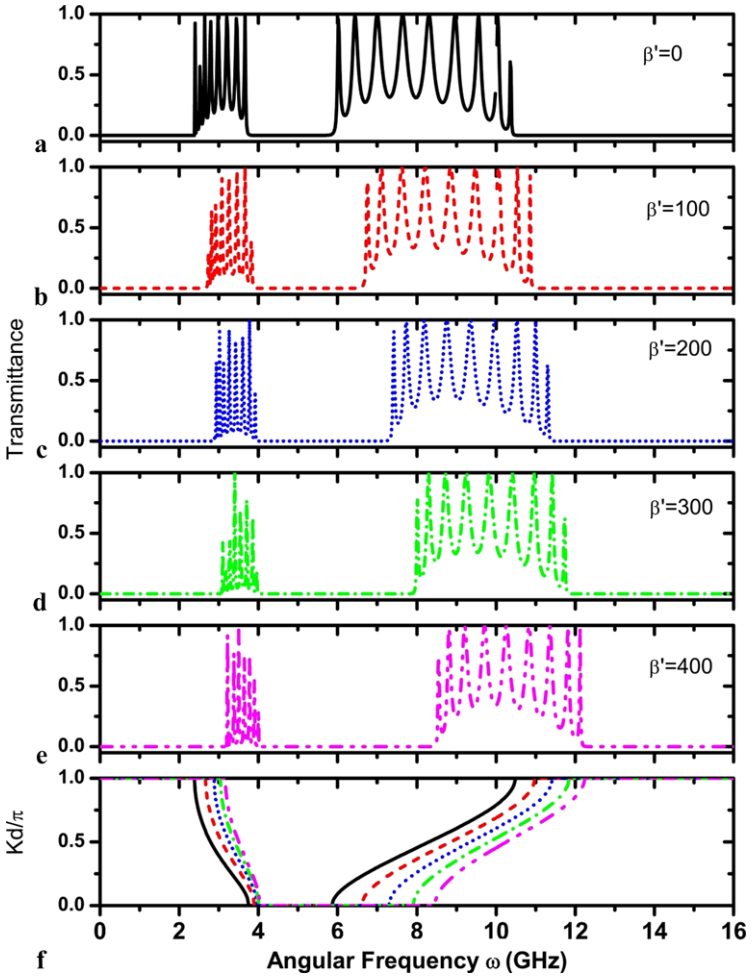

Fig. 7 Transmittance spectra (**a**)–(**e**) and the corresponding dispersion curve (**f**) for the one-dimensional ternary photonic crystals PC $(ACB)^M$ at different β'. (**a**) $\beta' = 0$, (**b**) $\beta' = 100$, (**c**) $\beta' = 200$, (**d**) $\beta' = 300$, and (**e**) $\beta' = 400$, the unit of β' is $(GHz)^2$, where $\alpha' = 0$, $d_C = 6$ mm, $\varepsilon_3 = 1$, and $\mu_3 = 1$, the other parameters have the same values as those in Fig. 3(b)

tonic band-edges formula in (17), the upper and lower band-edges frequencies should be rewritten as

$$\omega_1(\bar{\varepsilon} = 0) = \sqrt{\frac{\alpha + (d_C/d_A)\alpha'}{\varepsilon_1 + (d_B/d_A)\varepsilon_2 + (d_C/d_A)\varepsilon_3}}, \tag{25a}$$

$$\omega_2(\bar{\mu} = 0) = \sqrt{\frac{\beta + (d_C/d_B)\beta'}{\mu_2 + (d_A/d_B)\mu_1 + (d_C/d_B)\mu_3}}. \tag{25b}$$

Comparing (25) with (21), it is found that the denominators have the same form, but in the new equations, ε_3 and μ_3 cannot be negative. Moreover, the numerators has the new terms about α' and β' in (25). When $\alpha' = 0$ and $\beta' = 0$, (25) will recover to the band-edges formula (21) for the nondispersive material C. Now, we can discuss the schemes for extending the zero-φ_{eff} PBG in the new circumstance. In order to simplify the analysis, we set $\varepsilon_3 = \mu_3 = 1$. Hence, we can also get the two schemes for achieving the greater bandwidth $\Delta\omega = |\omega_1 - \omega_2|$ according to (25):

(a) When $\omega_1 < \omega_2$, to obtain larger width $\Delta\omega$, we should have smaller α' and larger β', which will decrease ω_1 and increase ω_2;

(b) When $\omega_1 > \omega_2$, to obtain larger width $\Delta\omega$, we should have larger α' and smaller β', which will increase ω_1 and decrease ω_2.

According to the scheme (a), we can set $\alpha' = 0$, hence the lower frequency limit $(\omega_1(\bar{\varepsilon} = 0))$ keeps fixed and the upper frequency limit $(\omega_2(\bar{\mu} = 0))$ increases if we increase β'. Combined these conditions with (24), it is found that at the same frequencies the greater value of β' is, the more negative value of μ_C is. Hence, the material C shows the nature of the MNG material. Similarly, according to the scheme (b), we can set $\beta' = 0$, the lower frequency limit $(\omega_2(\bar{\mu} = 0))$ keeps fixed and the upper frequency limit $(\omega_1(\bar{\varepsilon} = 0))$ increases if we increase α'. Then in this scheme, the material C shows the nature of the ENG material. And the greater value of α' is, the more negative value of ε_C is.

Firstly, we consider the scheme (a), the dependences of the transmittance spectra on the different β' have been shown in Fig. 7, where we have set $\varepsilon_3 = \mu_3 = 1$, $\alpha' = 0$. To assure the condition $\omega_1(\bar{\varepsilon} = 0) < \omega_2(\bar{\mu} = 0)$, we assume that $d_B = 24$ mm, the other parameters in the materials A and B have the same values as those in the Fig. 2. Figure 7(a) shows the transmittance spectra of the binary PC.

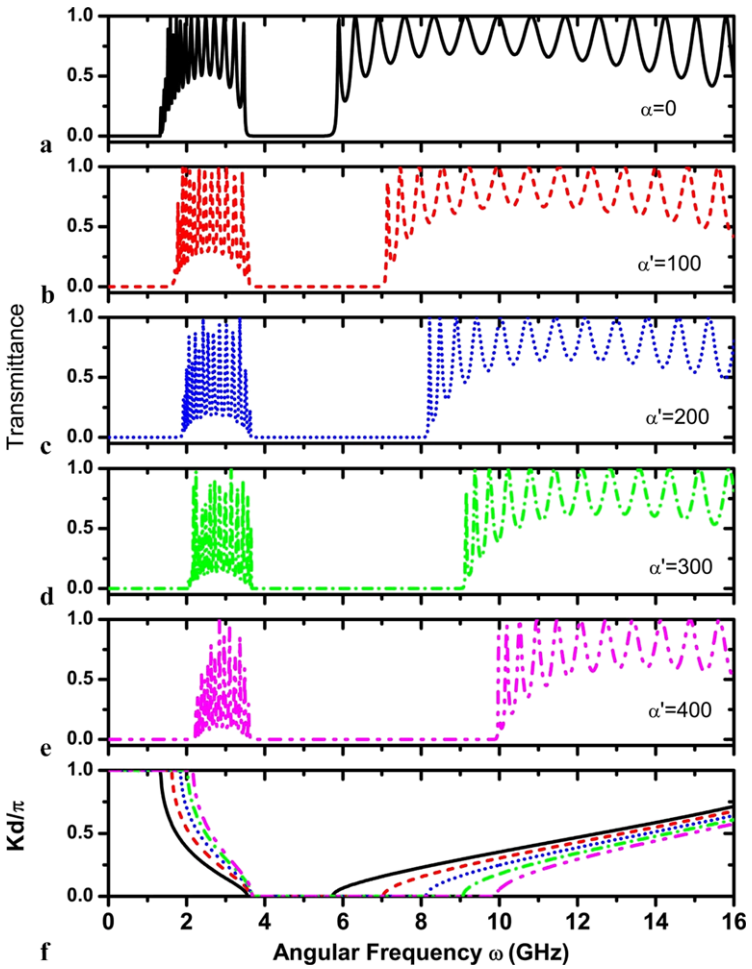

Fig. 8 Transmittance spectra (**a**)–(**e**) and the corresponding dispersion curve (**f**) for the one-dimensional ternary photonic crystals PC $(ACB')^M$ at different α'. (**a**) $\alpha' = 0$, (**b**) $\alpha' = 100$, (**c**) $\alpha' = 200$, (**d**) $\alpha' = 300$, and (**e**) $\alpha' = 400$, the unit of α' is $(\text{GHz})^2$, where $\beta' = 0$, $d_C = 6$ mm, $\varepsilon_3 = 1$, and $\mu_3 = 1$, the other parameters have the same values as those in Fig. 3(a)

Obviously, as the sandwiching of the layer C, the lower frequency limits have remained almost the same, however the upper frequency limits shift to higher frequency continually with the increasing β'. These results cause the widths of the bandgaps increasing continuously as the increasing β'. Here, the larger β' means more negative μ_C, which has similar nature with the scheme (1) in the non-dispersive layer C.

Next, we discuss the scheme (b), here we assume that $d_B = 6$ mm, and the other parameters on the materials A and B have the same values as those in the Fig. 7, which is calculated under $\omega_1(\bar{\varepsilon} = 0) > \omega_2(\bar{\mu} = 0)$. The dependences of the transmittance spectra on the different α' have been shown in the Fig. 8, where we have set $\varepsilon_3 = \mu_3 = 1$, $\beta' = 0$. Similar to the scheme (a), the upper frequency limits shift to the higher frequency as the increasing α', and at the same time the width of the bandgap becomes larger and larger. Here, the bigger α' means more negative ε_C, this scheme has akin properties with the scheme (2) in the nondispersive layer C. Comparing the scheme (b) with scheme (a), it is clear that we can obtain wider width of the zero-φ_{eff} PBG in the scheme (b) at the same conditions.

4 Conclusion

In summary, the band-edges formula for the one-dimensional ternary photonic crystal is derived based on the effective-medium theory and the expressions of the upper and lower frequency limits for the ternary photonic crystals are obtained. Then we presented two schemes to enlarge the zero-effective-phase (zero-φ_{eff}) bandgaps in the one-dimensional ternary photonic crystals. It is found that the gap width can be enhanced remarkably by sandwiching the layer C between two single-negative materials. Moreover, the enhancement factor can be continually increased by tuning the permittivity, permeability, and the thickness of the layer C. Finally, the angle- and polarization-dependence of the PBGs have been investigated. It is found that the omnidirectional PBG width of the zero-φ_{eff} PBG in the ternary PC is almost the two times as the width in the binary PC. Finally, the role of the dispersion in the sandwiching layer on the bandgap extending is discussed. It is found that the zero-φ_{eff} PBG can still be extended remarkably when we increase the electric or magnetic plasma frequencies. In that case, such an omnidirectional and wider bandwidth PBGs will offer many

prospects for omnidirectional optical switches, optical filters, and other optical devices in the future optical communication.

Acknowledgements We are grateful to the anonymous referee for insightful comments. This work is partially supported by the National Natural Science Foundation of China (Grants 11004053, 10974049, and 61025024), and the Fundamental Research Funds for the Central Universities.

References

1. E. Yablonovitch, Phys. Rev. Lett. **58**, 2059 (1987)
2. S. John, Phys. Rev. Lett. **58**, 2486 (1987)
3. N. Winn, Y. Fink, S. Fan, J.D. Joannopoulos, Opt. Lett. **23**, 1573 (1998)
4. Y. Fink, J.N. Winn, S. Fan, C. Chen, J. Michel, J.D. Joannopoulos, E.L. Thomas, Science **282**, 1679 (1998)
5. D.N. Chigrin, A.V. Lavrinenko, D.A. Yarotsky, S.V. Gaponenko, Appl. Phys. A **68**, 25 (1999)
6. A. Mir, A. Akjouj, E.H. El Boudouti, B. Djafari-Ronhani, L. Dobrzynski, Vacuum **63**, 197 (2001)
7. V.G. Veselago, Sov. Phys. Usp. **10**, 509 (1968)
8. V.M. Shalaev, Nat. Photonics **1**, 41 (2007)
9. J.B. Pendry, Phys. Rev. Lett. **85**, 3966 (2000)
10. J.S. Li, L. Zhou, C.T. Chan, P. Sheng, Phys. Rev. Lett. **90**, 083901 (2003)
11. D. Bria, B. Djafari-Rouhani, A. Akjouj, L. Dobrzynski, J.P. Vigneron, E.H. El Boudouti, A. Nougaoui, Phys. Rev. E **69**, 066613 (2004)
12. H.T. Jiang, H. Chen, H.Q. Li, Y.W. Zhang, S.Y. Zhu, Appl. Phys. Lett. **83**, 5386 (2003)
13. Y.J. Xiang, X.Y. Dai, S.C. Wen, D.Y. Fan, Phys. Rev. E **76**, 056604 (2007)
14. Y.J. Xiang, X.Y. Dai, S.C. Wen, D.Y. Fan, Opt. Lett. **33**, 1255 (2008)
15. H.T. Jiang, H. Chen, H.Q. Li, Y.W. Zhang, J. Zi, S.Y. Zhu, Phys. Rev. E **69**, 066607 (2004)
16. L.G. Wang, H. Chen, S.Y. Zhu, Phys. Rev. B **70**, 245102 (2004)
17. Y.J. Xiang, X.Y. Dai, S.C. Wen, D.Y. Fan, J. Opt. Soc. Am. A **24**, A28 (2007)
18. N. Krumbholz, K. Gerlach, F. Rutz, M. Koch, R. Piesiewicz, T. Kürner, D. Mittleman, Appl. Phys. Lett. **88**, 202905 (2006)
19. V. Kochergin, *Omnidirectional Optical Filters* (Kluwer, Norwell, 2003)
20. Y.H. Lu, M.D. Huang, S.Y. Park, P.J. Kim, T.-U. Nahm, Y.P. Lee, J.Y. Rhee, J. Appl. Phys. **101**, 036110 (2007)
21. H.Y. Zhang, Y.P. Zhang, W.H. Liu, Y.Q. Wang, J.G. Yang, Appl. Phys. B **96**, 67 (2009)
22. S.K. Awasthi, U. Malaviya, S.P. Ojha, J. Opt. Soc. Am. B **23**, 2566 (2006)
23. M. Born, E. Wolf, *Principles of Optics*, 7th (expanded) edn. (Cambridge University Press, Cambridge, 1999).
24. P. Yeh, *Optical Waves in Layered Media* (Wiley, New York, 1998)
25. D.R. Smith, D. Schurig, Phys. Rev. Lett. **90**, 077405 (2003)
26. S.M. Wang, C.J. Tang, T. Pan, L. Gao, Phys. Lett. A **351**, 391 (2006)
27. E. Silvestre, R.A. Depine, M.L. Martínez-Ricci, J.A. Monsoriu, J. Opt. Soc. Am. B **26**, 581 (2009)
28. J.A. Monsoriu, R.A. Depine, M.L. Martínez-Ricci, E. Silvestre, P. Andrés, Opt. Lett. **34**, 3172 (2009)